Progress In Electromagnetics Research, PIER 90, 385–407, 2009

ELECTROMAGNETIC ANALYSIS OF A NON INVASIVE MICROWAVE RADIOMETRY IMAGING SYSTEM EMPHASIZING ON THE FOCUSING SENSITIVITY OPTIMIZATION

M. I. Giamalaki, I. S. Karanasiou, and N. K. Uzunoglu

Microwave and Fiber Optics Laboratory
Department of Electrical and Computer Engineering
National Technical University of Athens
Greece

Abstract—A Green's function based methodology has been developed and implemented with the view to optimize the focusing properties and thus the performance of a Microwave Radiometry Imaging System (MiRaIS). The system consists of an ellipsoidal conductive wall cavity and a sensitive radiometric receiver and its operation principal is based on the convergence of the radiation from one focal point, where the subject or phantom is placed, on the other, where the receiver antenna is positioned. A two-layered cylinder is used to model the human head with the semi-analytical Green's function technique. The imaging configuration is enhanced by different matching structures of various materials which are placed on the surface of both the human head model and the antenna inside the ellipsoidal. Numerical code executions have been realized and the results for the electric field distribution inside the head are presented for materials of various dielectric properties and for left handed materials at two different frequencies (0.5 GHz and 1.0 GHz). Increased sensitivity of the system focusing properties is observed using particular matching structures.

1. INTRODUCTION

A potential medical imaging technique with a totally passive and non-invasive character is being developed over the past few years in the Microwave and Fiber Optics Lab of the National Technical University of Athens. The proposed imaging system operates at low microwave

Corresponding author: N. K. Uzunoglu (nuzu@cc.ece.ntua.gr).

frequencies and mainly consists of an ellipsoidal conductive cavity and a multifrequency sensitive radiometric receiver (Fig. 1) [1, 2]. The system operation principle is microwave radiometry through the detection of the chaotic radiation emitted by any material object, being at a temperature above the absolute zero, placed at one focal point of the ellipsoidal, by the receiver, placed at the other.

The novelty of the proposed imaging method lies on the use of the ellipsoidal cavity which due to its geometrical properties, provides convergence of the radiated electromagnetic energy from the area of interest of the human brain placed on one focal point, on the other focus where the receiver is placed.

Extensive phantom experiments as well as human tests have been realized in a non invasive, totally passive contactless manner and have shown promising results concerning the system's ability of detecting temperature and conductivity variation distributions [2–7].

The main scope of the present research with the view to assess its clinical value is to theoretically investigate the ability to image the specific cortical area of interest with the desired spatial resolution and detection depth. Thus in this paper various setups enhancing the system's focusing properties are theoretically studied. In previous studies, the implementation of dielectric materials as matching materials placed around the receiving antenna and/or the human head model to cause a stepped change of the refraction index on the scattering objects-air interface has been explored. Specifically, in order to achieve focusing improvement initially the receiving antenna was covered by two layers of different dielectric properties [8] and then a thin lossless dielectric layer was placed on the surface of the human head model [9].

Towards the enhancement of the system's focusing properties and overall performance, in the present paper new approaches have been

Figure 1. The existing microwave imaging system.

theoretically tested to implement a theoretical electromagnetic analysis based on the Green's function technique and all system attributes in terms of spatial resolution and detection depth are being calculated. A significant number of code executions have been conducted for various setups including different values of the thicknesses and the dielectric properties of the matching layers with a view to assess focusing optimization inside the brain. Moving on to a further stage a thin dielectric layer consisting of left handed material (metamaterial) has been also placed on the surface of the human head model for further focusing improvement. By this way the transition of the diffraction index from air to the head tissues and vice versa is attempted to be improved.

Numerical results for the electric field distribution inside the head model, derived by electromagnetic theoretical analysis, are presented for different operating frequencies in order to evaluate the benefits of the use of the above mentioned matching setups.

2. MATERIALS AND METHODS

2.1. System Overview

The Microwave Radiometry Imaging System consists of a conductive wall ellipsoidal reflector for focusing, a radiometric receiver and a data acquisition and processing system. The radiometric receiver consists of a microwave total power four-frequency-band radiometer and relevant broadband discone antenna operating in the range 1.0–3.1 GHz. The ellipsoidal cavity is made of fibreglass and has an inner highly conductive nickel coating. During the measurement procedure, the person or phantom is inserted inside the ellipsoidal through an opening and the region under measurement is placed at the focal point. The emitted energy is detected by the antenna placed on the other focus through reflection on the ellipsoidal conductive walls. The signal is then fed to the receiver followed by the pc for the data process.

According to previous experimental results the system shows the ability of measuring temperature and conductivity variations in phantoms and biological tissues [2–7]. Water phantom and animal experiments demonstrate that the voltage output from the system is linearly correlated with the actual temperature of the subjects of interest, a fact that is expected when the conductivity of the media under measurement remains unchanged [2–5, 7]. Experimental data from cylindrical shaped saline or de-ionized water filled tank phantoms, in which saline solutions of different concentrations were infused, provide promising results concerning the systems capability of detecting conductivity variations in phantoms at 3.5 GHz [6].

It is worth noticing that the data analysis from experiments involving the use of the proposed system with the participation of healthy volunteers indicates the potential value of using focused microwave radiometry to identify brain activation mechanisms potentially attributed to brain tissue conductivity changes.

The system design has been based on rigorous theoretical analysis that has been performed using commercial tools using FEM and FDTD and a semi-analytical method based on Greens function theory [1–4]. The field distribution inside the whole ellipsoidal volume as well as inside human head volumes has been calculated in detail and presented. An indicative result of the field distribution inside the whole ellipsoidal volume at 1.5 GHz is depicted in Fig. 2.

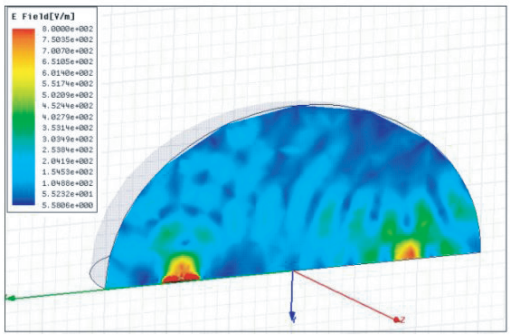

Figure 2. The field distribution in the whole elliptic chamber.

The aim of the present paper, as stated above, is the theoretical investigation of the optimization and enhancement of the system focusing attributes using different matching structures of various materials, such as lossless dielectric and left-handed materials, placed on the surface of both the human head model and the antenna inside the ellipsoidal at two operational frequencies.

2.2. Theoretical Electromagnetic Analysis

This paper includes a number of different setups in order to improve the system's focusing properties. The electromagnetic analysis is presented for the case when the receiving antenna is covered by two layers of different dielectric properties and a lossless dielectric layer is placed on the surface of the human head model. The rest of the investigated setups may be derived from this analysis by imposing the appropriate values for the dielectric properties and dimensions of the matching objects used.

The geometry of the problem is depicted in Fig. 3. A Cartesian coordinate system is used with origin at the point of section of the major and minor axes of the ellipse. The head is modeled by a double-layered cylinder with radii b_1 and b_2. These two layers are used to simulate different biological media; bone and brain (gray matter) tissues. The head model is surrounded by a cylinder with radii b_3. This extra portion is used in order to improve the transition of the diffraction index at the interface between air and human head. The center of the head is placed on a selected point (x_b, y_b) close to one of the ellipse's focal point.

The system is excited by two parallel linear current sources of infinite length and opposite sign (used to model the dipole antenna) which are surrounded by a double-layered cylinder with radii a_1 and a_2 whose center is placed on a selected point (x_a, y_a) close to the second focal point of the ellipsoidal reflector having a distance D from the center of the human head model. The dielectric properties of this double-layered cover are similar to those of the head. The sources' axes are considered parallel to z-axis.

The ellipse is defined by the following equation:

$$\frac{x^2}{a^2} + \frac{y^2}{b^2} = 1 \tag{1}$$

The interior of the ellipse is filled with air having wavenumber $k_0 = \omega\sqrt{\varepsilon_0\mu_0}$, where ω is the radian frequency, ε_0 and μ_0 are the free-space permittivity and permeability, respectively. In order to solve this problem, a Green's function technique is adopted [10–16]. According to the Reciprocity theorem, a response of a system to a source is unchanged when source and measurer are interchanged. Hence, instead of placing the source in the head model, the response of the head model,

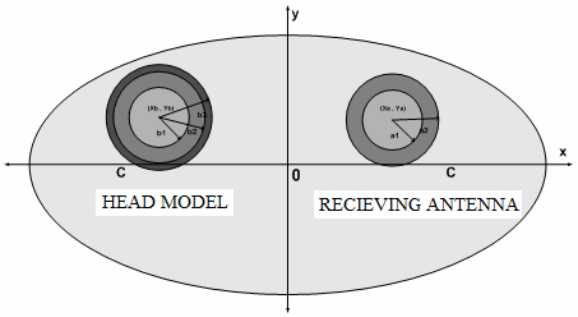

Figure 3. The geometry of the problem.

placed on one focal point of the ellipsoidal cavity, to the excitation generated by the antenna, positioned on the other focus, is calculated.

In the following analysis the sources surrounded by the double-layered cylinder are initially examined as an independent problem (Fig. 4). Green's function in each region $i = 1, 2, 3$ of space is properly expanded to an infinite sum of cylindrical waves satisfying the appropriate vector wave equation.

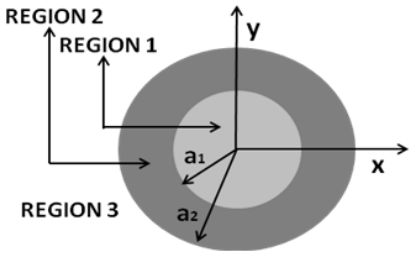

Figure 4. The sources surrounded by a double-layered cylinder.

The origin of the coordinate system used is the center of the cylinder as shown in Fig. 4. By virtue of the cylindrical symmetry of the problem, cylindrical coordinates are used, with unit vectors $\widehat{p}_a$ and $\widehat{\phi}_a$. The sources are located in two selected points with cylindrical coordinates p_1' and φ_1' and p_2' and φ_2'. The following expressions describe the electric-type Green's function in the three regions of space. Region 1 demonstrates the area inside the internal cylinder, Region 2 demonstrates the area inside the external cylinder and finally Region 3 demonstrates the area between the cylindrical model and the ellipsoidal.

Region 1:

$$G_1\left(\vec{p}_a\right) = \sum_{k=-\infty}^{\infty} a_k J_k\left(k_0 n_{a1} \vec{p}_a\right) e^{jk\phi_\alpha} + G_{01}\left(\vec{p}_a, \vec{p}\,'_1\right) + G_{02}\left(\vec{p}_a, \vec{p}\,'_2\right) \quad (2)$$

where $G_{01}(\vec{p}_a, \vec{p}\,'_1)$ and $G_{02}(\vec{p}_a, \vec{p}\,'_2)$, the contributions of the two sources are given by the following expression:

$$G_{01}\left(\vec{p}_a, \vec{p}\,'_1\right) = -\frac{j}{4} \sum_{k=-\infty}^{\infty} J_k(k_0 n_{a1} p_<) H_k^{(2)}(k_0 n_{a1} p_>) e^{jk(\phi-\phi_1)} \quad (3)$$

$$G_{02}\left(\vec{p}_a, \vec{p}\,'_2\right) = -e^{j\delta} \frac{j}{4} \sum_{k=-\infty}^{\infty} J_k(k_0 n_{a1} p_<) H_k^{(2)}(k_0 n_{a1} p_>) e^{jk(\phi-\phi_2)} \quad (4)$$

where $p_< = \min(p_a, p_1')$ and $p_> = \max(p_a, p_2')$

Region 2:

$$G_2(\vec{p}_a) = \sum_{k=-\infty}^{\infty} \left[b_k J_k \left(k_o n_{a2} \vec{p}_a \right) + b_k' Y_k \left(k_0 n_{a2} \vec{p}_a \right) \right] e^{jk\phi_\alpha} \tag{5}$$

Region 3:

$$G_3(\vec{p}_a) = \sum_{k=-\infty}^{\infty} c_k H_k^{(2)} \left(k_0 \vec{p}_a \right) e^{jk\phi_a} \tag{6}$$

where a_k, b_k, b_k' and c_k are unknown coefficients to be determined, $n_{ai} = \sqrt{\varepsilon_i}$, $J_k(k_0 n_{ai} \vec{p}_a)$ is the Bessel function of first kind, $Y_k(k_0 n_{ai} \vec{p}_a)$ is the Bessel function of second kind and $H_k^{(2)}(k_0 n_{ai} \vec{p}_a)$ is the Bessel function of third kind (Hankel function).

Hereupon, the unknown coefficients of the infinite sum of cylindrical waves are determined by the boundary conditions on the interfaces $p_a = a_1, a_2$. In order to satisfy the continuity of the electric and magnetic fields, the boundary conditions on the interfaces $p_a = a_1, a_2$ are then imposed by implementing the expressions:

$$G_i \left(\vec{p} \right) = G_{i+1} \left(\vec{p} \right) \qquad \vec{p} = a_i, \quad i = 1, 2 \tag{7}$$

$$\frac{\partial}{\partial p} \left(G_i \left(\vec{p} \right) \right) = \frac{\partial}{\partial p} \left(G_{i+1} \left(\vec{p} \right) \right) \qquad \vec{p} = a_i, \quad i = 1, 2 \tag{8}$$

By implementing the orthogonality properties of the cylindrical functions, the following four equations are obtained for the unknown coefficients stated above:

$$\begin{aligned} & -\frac{j}{4} J_k(k_0 n_{a1} d_1) H_k^{(2)}(k_0 n_{a1} a_1) \, e^{-jk\phi_1} \\ & -\frac{j}{4} e^{j\delta} J_k(k_0 n_{a1} d_2) H_k^{(2)}(k_0 n_{a1} a_1) \, e^{-jk\phi_2} + a_k J_k \left(k_0 n_{a1} a_1 \right) \\ = \; & b_k J_k \left(k_0 n_{a2} a_1 \right) + b_k' Y_k \left(k_0 n_{a2} a_1 \right) \end{aligned} \tag{9}$$

$$\begin{aligned} & -\frac{j}{4} J_k \left(k_0 n_{a1} d_1 \right) H_k'^{(2)} \left(k_0 n_{a1} a_1 \right) n_{a1} e^{-jk\phi_1} \\ & -\frac{j}{4} e^{j\delta} J_k \left(k_0 n_{a1} d_2 \right) H_k'^{(2)} (k_0 n_{a1} a_1) n_{a1} e^{-jk\phi_2} + a_k J'_k \left(k_0 n_{a1} a_1 \right) n_{a1} \\ = \; & b_k J'_k \left(k_0 n_{a2} a_1 \right) n_{a2} + b_k' Y_k' \left(k_0 n_{a2} a_1 \right) n_{a2} \end{aligned} \tag{10}$$

$$b_k J_k \left(k_0 n_{a2} a_2 \right) + b_k' Y_k \left(k_0 n_{a2} a_2 \right) = c_k H_k^{(2)} \left(k_0 a_2 \right) \tag{11}$$

$$b_k J_k' \left(k_0 n_{a2} a_2 \right) n_{a2} + b_k' Y_k' \left(k_0 n_{a2} a_2 \right) n_{a2} = c_k H_k'^{(2)} \left(k_0 a_2 \right) \tag{12}$$

The four unknown coefficients a_k, b_k, b'_k and c_k can be obtained with very low computational cost, so it is evident that the Green's function can be calculated at any point inside and outside the cylinders.

Moving on to the further stage all the system is examined using a new coordinate system which has origin at the center of the triple-layered cylinder that represents the head model covered by a matching layer (Fig. 5). By virtue of the cylindrical symmetry of the problem, cylindrical coordinates are used, with unit vectors $\widehat{p}_b$, $\widehat{\phi}_b$.

The following expressions describe the electric-type Green's functions in the four regions of space. Region 1 demonstrates the area inside the internal cylinder, Region 2 the area inside the middle cylinder, Region 3 the area inside the external cylinder which represents the matching layer and finally Region 4 the area between the cylindrical model and the ellipsoidal.

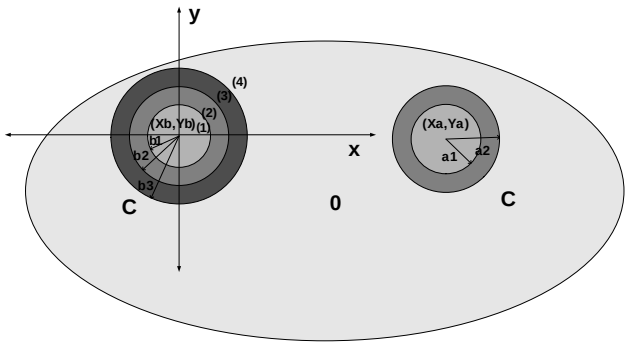

Figure 5. The coordinate system with origin the center of the triple-layered cylinder.

Region 1:

$$\Psi_1(\vec{p}_b) = \sum_{k=-\infty}^{\infty} q_k J_k(k_0 n_{b1} \vec{p}_b)\, e^{jk\phi_b} \tag{13}$$

Region 2:

$$\Psi_2(\vec{p}_b) = \sum_{k=-\infty}^{\infty} [S_k J_k(k_0 n_{b2} p_b) + W_k Y_k(k_0 n_{b2} p_b)] e^{jk\phi_b} \tag{14}$$

Region 3:

$$\Psi_3(\vec{p}_b) = \sum_{k=-\infty}^{\infty} [U_k J_k(k_0 n_{b3} p_b) + V_k Y_k(k_0 n_{b3} p_b)] e^{jk\phi_b} \tag{15}$$

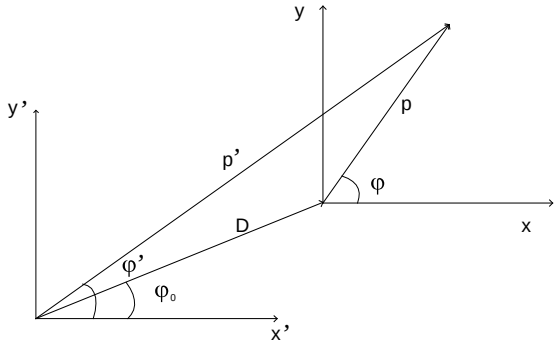

Figure 6. The coordinate systems used in the presented analysis.

Region 4:

$$\Psi_4(\vec{p}_b) = \sum_{k=-\infty}^{\infty} [r_k J_k(k_0 p_b) + t_k Y_k(k_0 p_b)] e^{jk\phi_b} + G_{3ad} \tag{16}$$

where G_{3ad} is $G_3(\vec{p}_a) = \sum_{k=-\infty}^{\infty} c_k H_k^{(2)}(k_0 \vec{p}_a) e^{jk\phi_a}$ for the new coordinate system and must be determined. Generally the following expressions are used:

$$H_k^{(2)}(k_0 p) e^{jk\phi} = \sum_{\lambda} H_{\lambda-k}^{(2)}(k_0 D) e^{-j(\lambda-k)\phi_0} J_\lambda\left(k_0 p'\right) e^{j\lambda\phi'} \text{ for } p' < D \quad (A)$$

$$H_k^{(2)}(k_0 p) e^{jk\phi} = \sum_{\lambda} J_{\lambda-k}(k_0 D) e^{-j(\lambda-k)\phi_0} H_\lambda^{(2)}\left(k_0 p'\right) e^{j\lambda\phi'} \text{ for } p' > D \quad (B)$$

where p, φ the cylindrical coordinates of the initial system, p', φ' the cylindrical coordinates of the new system, D the distance between the origin of the initial and the origin of the new system and φ_0 the angle from the new system to the initial as shown in Fig. 6.

In our case expression (A) for $p' < D$ will be used because it is necessary in order to satisfy the boundary condition between Regions 3 and 4 where $p_b = b_3$ which is $< D$. In this way the expression for G_{3ad} will be:

$$G_{3ad} = \sum_k c_k \sum_\lambda H_{\lambda-k}^{(2)}(k_0 D) e^{-j(\lambda-k)\phi_0} J_\lambda(k_0 p_b) e^{j\lambda\phi'} \tag{17}$$

Following the unknown coefficients q_k, S_k, W_k, U_k, V_k, r_k, t_k are determined by the boundary conditions on the interfaces $p_b =$

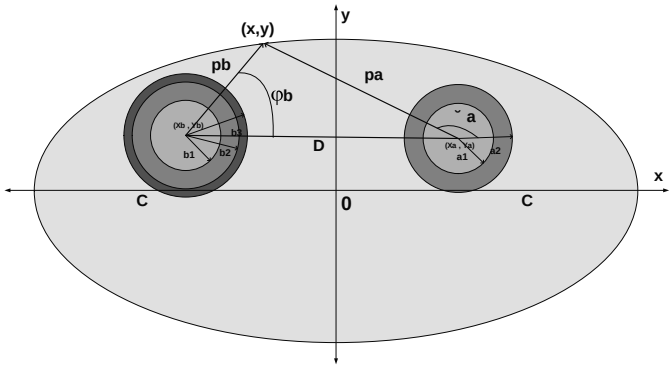

Figure 7. The triple-layered model of the human head and the matching layer placed on a selected point $(x_b,\ y_b)$, the sources surrounded by the double-layered cylinder placed on a selected point $(x_a,\ y_a)$ and the central coordinate system.

b_1, b_2, b_3. Working as before, the following six linear equations are obtained for the unknown coefficients stated above.

$$q_k J_k\left(k_0 n_{b1} b_1\right) = S_k J_k\left(k_0 n_{b2} b_1\right) + W_k Y_k\left(k_0 n_{b2} b_1\right) \tag{18}$$

$$q_k J'_k\left(k_0 n_{b1} b_1\right) n_{b1} = S_k J'_k\left(k_0 n_{b2} b_1\right) n_{b2} + W_k Y'_k\left(k_0 n_{b2} b_1\right) n_{b2} \tag{19}$$

$$S_k J_k\left(k_0 n_{b2} b_2\right) + W_k Y_k\left(k_0 n_{b2} b_2\right) = U_k J_k(k_0 n_{b3} b_2) + V_k Y_k\left(k_0 n_{b3} b_2\right) \tag{20}$$

$$\begin{aligned} &S_k J'_k\left(k_0 n_{b2} b_2\right) n_{b2} + W_k Y'_k\left(k_0 n_{b2} b_2\right) n_{b2} \\ &= U_k J'_k(k_0 n_{b3} b_2) n_{b3} + V_k Y'_k\left(k_0 n_{b3} b_2\right) n_{b3} \end{aligned} \tag{21}$$

$$\begin{aligned} &U_k J_k\left(k_0 n_{b3} b_3\right) + V_k Y_k\left(k_0 n_{b3} b_3\right) = r_k J_k(k_0 b_3) + t_k Y_k(k_0 b_3) \\ &+ \sum_m c_m H^{(2)}_{k-m}(k_0 D) e^{-j(k-m)\phi_0} J_k(k_0 b_3) \end{aligned} \tag{22}$$

$$\begin{aligned} &U_k J'_k\left(k_0 n_{b3} b_3\right) n_{b3} + V_k Y'_k\left(k_0 n_{b3} b_3\right) n_{b3} = r_k J'_k\left(k_0 b_3\right) + t_k Y'_k\left(k_0 b_3\right) \\ &+ \sum_m c_m H^{(2)}_{k-m}\left(k_0 D\right) e^{-j(k-m)\phi_0} J'_k\left(k_0 b_3\right) \end{aligned} \tag{23}$$

Consequently, six linear equations are obtained for the seven unknown coefficients stated above. The remaining boundary condition to be imposed is on the conductive ellipse, where the electric field must be zero. Hence, a Cartesian coordinate system is used, with origin at the point of section of the major and minor axes of the ellipse as shown in Fig. 7.

The infinite sum with respect to k is convergent and hence it can be truncated to a finite one. The electric field on the ellipse must be

zero, so the following equation can be obtained:

$$\Psi_4(n_i) = \sum_{k=-\infty}^{+\infty} r_k \left[J_k(k_0 p_b) + z_k Y_k(k_0 p_b)\right] e^{jk\phi_b} + \sum_{k=-\infty}^{+\infty} P_k Y_k(k_0 p_b) e^{jk\phi_b} + G_3(p_a, \phi_a) = 0 \quad (24)$$

where

$$G_3(p_a, \phi_a) = \sum_{k=-N}^{N} c_k H_k^{(2)}(k_0 p_a) e^{jk\phi_a} \quad (25)$$

z_k and P_k are known coefficients that contain the six remaining coefficients: q_k, S_k, W_k, U_k, V_k, t_k and r_k is the only unknown coefficient. The infinite sum with respect to m in Equations (22) and (23) is convergent and hence it can be truncated to a finite one.

The estimation of the electric field is obtained from Equation (24) by assessing the only unknown coefficient r_k. The infinite sum with respect to n is convergent and, hence, it can be truncated to a finite one. Therefore, Equation (24) is applied on a mesh of $(2N+1)$ collocation points on the surface of the ellipsoidal so it can be equivalently written as:

$$\Psi_4(n_i) = \sum_{k=-N}^{N} r_k \left[J_k(k_0 p_b) + z_k Y_k(k_0 p_b)\right] e^{jk\phi_b} + \sum_{k=-N}^{N} P_k Y_k(k_0 p_b) e^{jk\phi_b} + G_3(p_a, \phi_a) = 0 \quad (26)$$

where

$$G_3(p_a, \phi_a) = \sum_{k=-N}^{N} c_k H_k^{(2)}(k_0 p_a) e^{jk\phi_a} \quad (27)$$

and N is the number of terms required for the convergence of the infinite sum.

The position of each collocation point is determined by the following expressions for p_a, φ_a, p_b, φ_b referring to the central coordinate system:

$$p_a = \sqrt{(a\cos n_i - x_a)^2 + (b\sin n_i - y_a)^2} \quad (28)$$

$$p_b = \sqrt{(a\cos n_i - x_b)^2 + (b\sin n_i - y_b)^2} \tag{29}$$

$$\phi_a = \tan^{-1}\frac{(b\sin n_i - y_a)}{(a\cos n_i - x_a)} \tag{30}$$

$$\phi_b = \tan^{-1}\frac{(b\sin n_i - y_b)}{(a\cos n_i - x_b)} \tag{31}$$

where

$$n_i = \frac{2\pi}{2N+1}i, \quad i = 0, \ldots, 2N \tag{32}$$

It is evident that the electric field can be calculated at any point inside the ellipse, inside and outside the human head model and inside and outside the double-layered cylinder that covers the source, with very low computational cost.

At this point, it must be taken into consideration that when the layer that covers the head model consists of metamaterial the expressions derived by Equation (8) for the satisfaction of the continuity of the magnetic field must change on the interfaces $p_b = b_2, b_3$. Consequently:

$$\frac{1}{\mu_0}\frac{\partial\Psi_2}{\partial\rho} = \frac{1}{\mu_3}\frac{\partial\Psi_3}{\partial\rho}$$
$$\frac{1}{\mu_3}\frac{\partial\Psi_3}{\partial\rho} = \frac{1}{\mu_0}\frac{\partial\Psi_4}{\partial\rho}$$

Hence, the following six equations are obtained for the unknown coefficients:

$$q_k J_k(k_0 n_{b1} b_1) = S_k J_k(k_0 n_{b2} b_1) + W_k Y_k(k_0 n_{b2} b_1) \tag{33}$$

$$q_k J_k'(k_0 n_{b1} b_1)\, n_{b1} = S_k J_k'(k_0 n_{b2} b_1)\, n_{b2} + W_k Y_k'(k_0 n_{b2} b_1)\, n_{b2} \tag{34}$$

$$S_k J_k(k_0 n_{b2} b_2) + W_k Y_k(k_0 n_{b2} b_2) = U_k J_k(k_0 n_{b3} b_2) + V_k Y_k(k_0 n_{b3} b_2) \tag{35}$$

$$S_k J'_k(k_0 n_{b2} b_2)\, n_{b2} + W_k Y_k'(k_0 n_{b2} b_2)\, n_{b2} = \frac{1}{M}(U_k J_k'(k_0 n_{b3} b_2) n_{b3} + V_k Y_k'(k_0 n_{b3} b_2)\, n_{b3}) \tag{36}$$

$$U_k J_k(k_0 n_{b3} b_3) + V_k Y_k(k_0 n_{b3} b_3) = r_k J_k(k_0 b_3) + t_k Y_k(k_0 b_3) + \sum_m c_m H_{k-m}^{(2)}(k_0 D)\, e^{-j(k-m)\phi_0} J_k(k_0 b_3) \tag{37}$$

$$U_k J'_k(k_0 n_{b3} b_3)\, n_{b3} + V_k Y_k'(k_0 n_{b3} b_3)\, n_{b3} = M\Big\{ r_k J_k'(k_0 b_3) + t_k Y_k'(k_0 b_3) + \sum_m c_m H_{k-m}^{(2)}(k_0 D)\, e^{-j(k-m)\phi_0} J_k'(k_0 b_3) \Big\} \tag{38}$$

where $M = \frac{\mu_3}{\mu_o}$.

In this way, six linear equations are obtained for the seven unknown coefficients stated above. The electric field on the ellipse must be zero; so working as before, Equation (26) can be obtained and since r_k is the only unknown coefficient, the electric field can be calculated at any point.

3. NUMERICAL RESULTS

The estimation of the electromagnetic field in the interior of a human head model placed in the area of the one focal point of the ellipsoidal cavity when the system is excited by a source placed in the other focal point is presented in this paper. In order to enhance the system's focusing properties the following matching setups are being analytically examined:

- The receiving antenna is covered by two layers of the same dimensions and dielectric properties as those of the head.
- The head model is covered by a matching layer having various values of dielectric properties and thickness.
- The human head model is surrounded by a dielectric layer consisting of left handed material of various values of thickness.

The problem was solved for two different frequencies $f_1 = 0.5\,\text{GHz}$ and $f_2 = 1.0\,\text{GHz}$. The dimensions of the ellipse used for the computation were $a = 75\,\text{cm}$ and $b = 60\,\text{cm}$ with inter focal distance $2c = 2\sqrt{a^2 - b^2} = 90\,\text{cm}$. These dimensions are in fact the actual dimensions of the ellipsoidal reflector that has been constructed in our laboratory.

The dielectric properties of the tissue composition used for the computation for the brain (gray matter) and for the skull at 0.5 GHz are shown in Table 1 and the respective values for the frequency of 1GHz are shown in Table 2 [17–19]. The head model, including skull and thick brain (gray matter) is of total diameter 16 cm with $b_1 = 7\,\text{cm}$ and $b_2 = 8\,\text{cm}$.

Table 1. The dielectric properties of the tissue composition for the frequency of 0.5 GHz.

0.5 GHz	ε	σ	n
For brain (grey matter)	$\varepsilon_1 = 48.417667$	$\sigma_1 = 0.626460$	$n_{b1} = \sqrt{48.417667\text{-}22.55256i}$
For skull	$\varepsilon_2 = 17.447731$	$\sigma_2 = 0.177212$	$n_{b2} = \sqrt{17.447731\text{-}6.379632i}$

Table 2. The dielectric properties of the tissue composition for the frequency of 1 GHz.

1.0 GHz	ε	σ	n
For brain (grey matter)	$\varepsilon_1 = 45.429596$	$\sigma_1 = 0.803625$	$n_{b1} = \sqrt{45.429596\text{-}14.46525i}$
For skull	$\varepsilon_2 = 16.473764$	$\sigma_2 = 0.259788$	$n_{b2} = \sqrt{16.473764\text{-}4.676184i}$

The total diameter of the double-layered cylinder that covers the sources is also 16 cm and $a_1 = 7$ cm, $a_2 = 8$ cm. The dielectric properties used for the computation are $n_{a1} = \sqrt{\varepsilon_1\mu_1}$ and $n_{a2} = \sqrt{\varepsilon_2\mu_2}$ where ε_1 and ε_2 are shown in the tables for each operating frequency, since its dielectric properties are chosen to be similar to those of the head (materials of the same dimensions and the same dielectric properties but lossless). This approach is followed in order to investigate whether similar setups in conjugate focuses will produce similar focusing performance. The magnetic properties of the head model's layers, the matching layer that covers the head and the layers that cover the source are denoted as $\mu_1 = \mu_2 = \mu_3 = \mu_0$.

3.1. The Receiving Antenna Is Covered by Two Matching Layers

The first case that is being examined is when the head is modeled by a double-layered cylinder and the system is excited by two linear sources covered by a double-layered cylinder. The solution can be achieved by apposing the proper changes to the numerical code that has been established for the solution of the above general problem. The focusing achieved inside the human head model, in relation each time to the area that is placed at the focal point is being examined. Initially, the centre of the double layered cylindrical head model is set at the first focal point while both the sources and the surrounding double layered cylinder centres are placed on the other focal point (case 1). Following more numerical code executions are conducted when the center of the head is moved left by 6 cm away from the focal point of the ellipse while the sources surrounded by the dielectric cylinder are kept still on the focal point (case 2).

These two distinct cases are examined for two main operating frequencies, 0.5 GHz and 1 GHz. The two current sources are placed in the centre of the dielectrics, having a distance of 0.01 m from one another. The number of terms required for the infinite sums to converge is $N = 14$ at 0.5 GHz and $N = 24$ at 1 GHz. These

numbers ensure convergence of the obtained solution at any point. The continuity of the fields at the $r = a_1$, a_2, b_1, b_2 between different layers has been checked and verified numerically. The validity of the boundary conditions on the ellipse has also been checked. The results of the computation are depicted in Fig. 8.

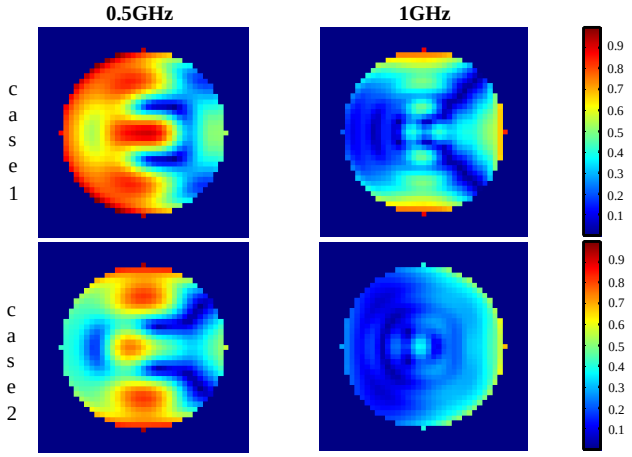

Figure 8. The field distribution inside the head model for the two cases at the two operating frequencies, when two sources are covered by two dielectric layers.

At the low frequency of 0.5 GHz it is observed that the penetration depth is high in both cases in contrast with the higher frequency of 1 GHz. In the second case the sensitivity of the system is tested in terms of placing a different area of the human head model at the focus: it is indeed observed that the field tends to converge to head areas which are placed closer to the ellipsoid's focus, depending on the penetration depth and the operation frequency.

3.2. The Head Model Is Covered by a Matching Layer of Dielectric Material

In order to assess the focusing optimization of the system in terms of spatial accuracy and detection depth the head which is modelled by a double-layered cylinder is in addition covered by an extra cylindrical layer when the two linear sources are covered by a double-layered cylinder. Numerical results are presented for the electric field distribution inside the head model for the same two scenarios investigated in the former case while more numerical code executions are conducted by moving the head model's centre vertically by 6 cm

away from the focal point at the frequencies of 0.5 GHz and 1 GHz. The two current sources are kept still on the other focal point at the centre of the dielectrics having a distance of 0.01 m from one another. The number of terms required for the infinite sums to converge is $N = 14$ at 0.5 GHz and $N = 24$ at 1 GHz. The continuity of the fields at the $r = a_1$, a_2, b_1, b_2, b_3 between different layers has been checked as well as the validity of the boundary conditions on the ellipse. Subsequently, several trials are conducted with a matching layer that covers the head model having two different dielectric properties ($n_{b3} = \sqrt{6}$ and $n_{b3} = \sqrt{12}$) while their thickness varies from 1 cm to 2 cm.

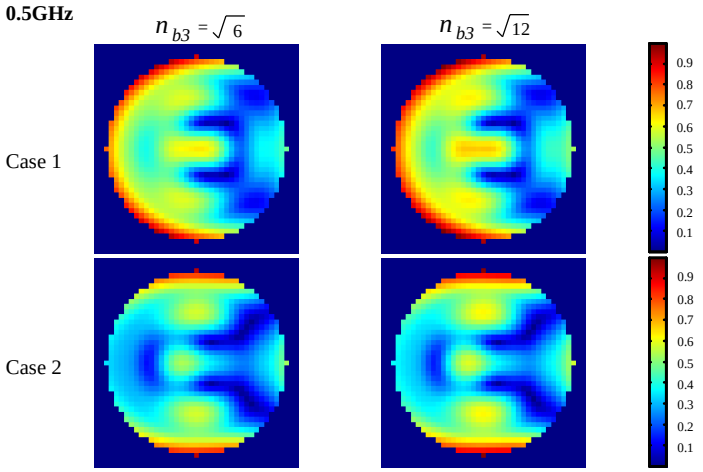

Figure 9. The field distribution inside the head model for the two cases at 0.5 GHz when the thickness of the matching layer is 1 cm.

The results of the computation depicted in Fig. 9 are for a matching layer of two different dielectric properties when its thickness is 1 cm at the frequency of 0.5 GHz. The two cases presented in the above figure are when the centre of the head model is set at the first focal point (case 1) and when the center of the head is moved left by 6 cm away from the focal point of the ellipse (case 2).

The results depicted in Figs. 10 and 11 are for a matching layer of two different dielectric properties and of two different thicknesses at the frequency of 0.5 GHz and 1 GHz respectively when the head is moved vertically by 6 cm.

At the low operational frequency it is observed that the penetration depth is high in all cases. When the dielectric layer is placed (n_{b3} is $\sqrt{12}$) a higher detection depth is achieved at both frequencies. An increased sensitivity in focusing is observed for both

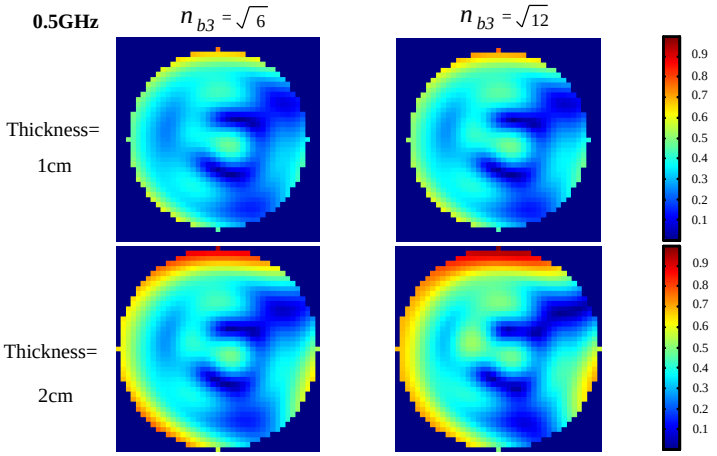

Figure 10. The field distribution inside the head model at 0.5 GHz when the matching layer has 1 cm or 2 cm thickness and n_{b3} is $\sqrt{6}$ or $\sqrt{12}$.

frequencies when moving the head away from the system's geometrical focal area. It should be noted that on the above figures the matching layers are also depicted and this is the reason why large field values appear on the surface of the head model. The figures from the

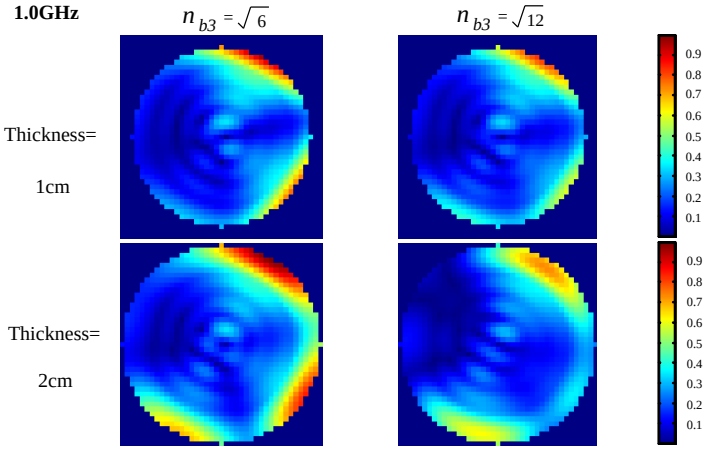

Figure 11. The field distribution inside the head model at 1 GHz when the matching layer has 1 cm or 2 cm thickness and n_{b3} is $\sqrt{6}$ or $\sqrt{12}$.

numerical results show that at the high frequency a matching layer of 1 cm is adequate to increase spatial sensitivity in terms of placement relative to the focus and at the same time ensure adequate detection depth. The use of a matching layer of 2 cm thickness does not provide any significantly improved outcome. At the lower frequency the thickness of the matching layer needs to be at least 2 cm in order to achieve a higher penetration depth (Fig. 11).

Consequently the results have shown improvement of the system attributes by using a lossless dielectric layer with dielectric permittivity value $\varepsilon_r = 12$, placed on the surface of the human head model. By this way the transition of the diffraction index from air to the head and vice versa is improved. Thus, the area of the head that is placed on the focal area of the ellipsoidal reflector can be measured with better accuracy.

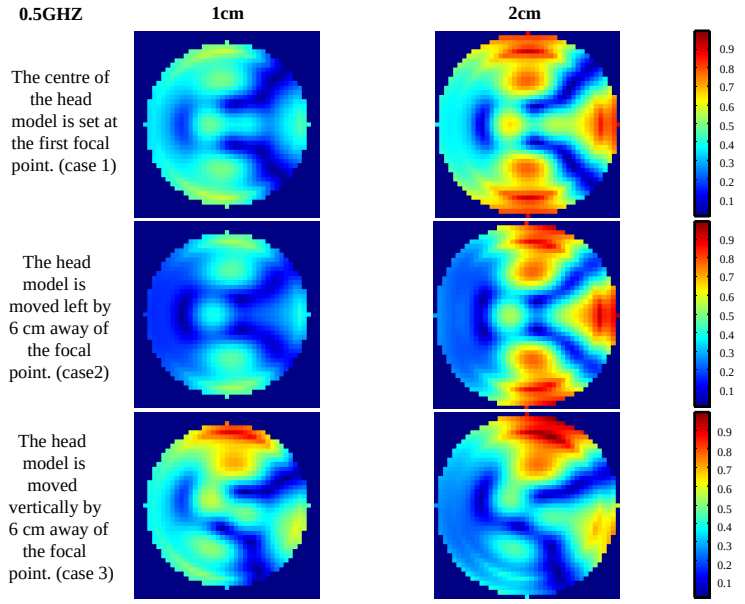

Figure 12. The field distribution inside a double-layered human head model, covered by a matching layer consisting of metamaterial, of two different thicknesses, 1 cm and 2 cm at 0.5 GHz.

3.3. The Head Model Is Covered by a Dielectric Layer Consisting of Left Handed Material

Following, our research focuses on placing a dielectric layer consisting of left handed material on the surface of the human head model for further focusing improvement [20–28]. The scenarios which are examined are when the centre of the head model is set at the first focal point while the sources are kept still on the other focal point (case 1) and when the head model is placed in various positions inside the ellipse (case 2), (case 3).

Calculations have been conducted for two different thicknesses 1 cm and 2 cm of the metamaterial layer at two different frequencies: 0.5 GHz and 1 GHz. The number of terms required for the convergence of the infinite sum N is 14 and 24 at the frequencies 0.5 GHz and 1 GHz respectively. The dielectric properties of the layer consisting of left handed material used for the numerical code execution are $\varepsilon = -1$ and $\mu = -1$. For M used at the above equations: $M = \frac{\mu_3}{\mu_0} = \frac{\mu \cdot \mu_0}{\mu_0} = -1$. Veselago in 1968 has shown that if ε and μ have negative values then for the diffraction index it applies that $n = -\sqrt{\varepsilon\mu}$. Hence the value of n_{b3} used for the computation is equal to -1 for the three operating frequencies.

The results from the numerical code executions presented in the following Fig. 12 show the field distribution inside the head model surrounded by a layer consisting of metamaterial of 1 cm and 2 cm thickness at the frequency of 0.5 GHz.

By observing the above figures it is concluded that the thickness of the matching layer seems to play an important role. In all cases examined above, an increased sensitivity in focusing is achieved when moving the head and it is observed on the anticipated side of the human head model. Thus when the head is moved either left or down, the field converges not on the centre of the head as when no matching dielectric or metamaterial layer is used but on the actual head region area placed at the focal point. For the higher frequency regarding the penetration depth and the system's focusing properties, it is concluded that the 2 cm thick layer of metamaterial surrounding the head model provides optimized results.

4. DISCUSSION AND CONCLUSIONS

The main scope of this research was the enhancement of the MiRaIS's focusing properties based on the results of a theoretical electromagnetic analysis performed when different matching structures were added to the system. Matching layers of different materials and thicknesses were

placed on the surface of both the head model and the antenna. Initially the receiving antenna was covered by two layers of dielectric properties similar to those of the head, then the human head model was covered by dielectric layers and finally the later was covered by dielectric layers consisting of left handed material.

In all the above cases it was observed that the higher was the penetration depth the lower was the frequency as expected. In addition it can be concluded that sensitivity of the system focusing properties was observed when the head was moved away from the system's geometrical focal area. By observing the results of the various simulation scenarios, it can be derived that with the usage of matching layers the bounds of the focusing area are better delimited and defined, whereas the penetration depth is also improved. In the case of a matching layer placed on the surface of the head model, improved system focusing attributes were achieved when its dielectric permittivity value was $\varepsilon_r = 12$ for all frequencies. Such a dielectric permittivity value seems to cause a stepped transition of the diffraction index from air to head and vice versa resulting in the larger penetration/detection depth. At 1 GHz operating frequency the thickness of such a matching layer was 1 cm while at 0.5 GHz the results show that it should be at least 2 cm thick. Finally the use of a metamaterial layer of 2 cm thickness surrounding the surface of the head model provides significantly optimized system focusing attributes at both frequencies. With negative permittivity and permeability simultaneously, the LHM seems to provide the desirable improvement of the systems detection depth and focusing.

Experiments with the optimized configurations will be conducted using a multiband sensitive receiver in order to verify the theoretical findings and investigate the foreseen system performance in detecting conductivity and/or temperature variations in phantoms and biological tissues.

ACKNOWLEDGMENT

The present work is supported by the General Secretariat of Research and Technology of the Hellenic Ministry of Development through the program PENED2003 (ΠΕΝΕΔ2003).

REFERENCES

1. Karanasiou, I. S., "Development of a non invasive brain imaging system using microwave radiometry," Doctor of Philosophy in

Engineering, School of Electrical and Computer Engineering, National Technical University of Athens, Dec. 2003 (in Greek).

2. Karanasiou, I. S., N. K. Uzunoglu, and C. Papageorgiou, "Towards functional non-invasive imaging of excitable tissues inside the human body using focused microwave radiometry," *IEEE Transactions on Microwave Theory and Techniques*, Vol. 52, No. 8, 1898–1908, Aug. 2004.
3. Karanasiou, I. S., N. K. Uzunoglu, and A. Garetsos, "Electromagnetic analysis of a non-invasive 3D passive microwave imaging system," *Progress In Electromagnetics Research*, PIER 44, 287–308, 2004.
4. Karanasiou, I. S., N. K. Uzunoglu, S. Stergiopoulos, and W. Wong, "A passive 3D imaging thermograph using microwave radiometry," *Innovation and Technology in Biology Medicine*, Vol. 25, 227–239, 2004.
5. Karanasiou, I. S. and N. K. Uzunoglu, "Development and feasibility study of a functional brain passive microwave tomography system," *URSI 2004 Proceedings*, 1194–1196, Pisa, Italy, 2004.
6. Karanasiou, I. S. and N. K. Uzunoglu, "Experimental study of 3D contactless conductivity detection using microwave radiometry: A possible method for investigation of brain conductivity fluctuations," *EMBC'04 Proceedings*, 2303–2306, San Fransisco, USA, 2004.
7. Karanasiou, I. S., M. I. Giamalaki, A. Oikonomou, and N. K. Uzunoglu, "Passive four-frequency microwave tomography: An experimental feasibility study," *IFMBE Proceedings*, Vol. 11, 2086-1–2086-5, Prague, 2005.
8. Giamalaki, M. I., I. S. Karanasiou, and N. K. Uzunoglu, "Enhancement of the focusing properties of a passive radiometry imaging system: A theoretical electromagnetic study," *ICEAA'07 Proceedings*, No. 263, Torino, Italy, 2007.
9. Giamalaki, M. I., I. S. Karanasiou, and N. K. Uzunoglu, "Focused microwave radiometry from a possible functional imaging perspective: Theoretical optimization of the properties of a microwave radiometry system," *ITBS 2007 Proceedings*, 36–37, Milos Island, Greece, 2007.
10. Acar, R. C. and G. Dural, "Mutual coupling of printed elements on a cylindrically layered structure using closed-form Greens functions," *Progress In Electromagnetics Research*, PIER 78, 103–127, 2008.
11. Gao, G., C. Torres-Verdin, and T. M. Habashy, "Analytical

techniques to evaluate the integrals of 3D and 2D spatial dyadic Greens functions," *Progress In Electromagnetics Research*, PIER 52, 47–80, 2005.

12. Li, L.-W., N.-H. Lim, and W.-Y. Yin, "Eigenfunctional expansion of dyadic Green's functions in gyrotropic media using cylindrical vector wave functions," *Progress In Electromagnetics Research*, PIER 43, 101–121, 2003.
13. Li, L.-W., S. B. Yeap, M. S. Leong, T. S. Yeo, and P. S. Kooi, "Dyadic Green's functions in multilayered stratified gyroelectric chiral media," *Progress In Electromagnetics Research*, PIER 35, 53–81, 2002.
14. Li, L.-W., N.-H. Lim, and J. A. Kong, "Cylindrical vector wave function representation of Green's dyadic in gyrotropic bianisotropic media," *Progress In Electromagnetics Research*, 127–145, 2008.
15. Attiya, M., "Dyadic Green's function of an elementary point source above a periodically-defected-grounded dielectric slab," *Progress In Electromagnetics Research B*, Vol. 4, 127–145, 2008.
16. Lamultree, S., C. Phongcharoenpanich, S. Kosulvit, and M. Krairiksh, "Analysis of radiation characteristics of a probe-excited rectangular ring antenna by the dyadic Green's function approach," *Progress In Electromagnetics Research B*, Vol. 11, 79–101, 2009.
17. Gabriel, C., S. Gabriel, and E. Corthout, "The dielectric properties of biological tissues: I. Literature survey," *Physics in Medicine and Biology*, Vol. 41, 2251–2269, 1996.
18. Gabriel, S., R. W. Lau, and C. Gabriel, "The dielectric properties of biological tissues: II. Measurements in the frequency range 10 Hz to 20 GHz," *Physics and Medicine and Biology*, Vol. 41, 2251–2269, 1996.
19. Gabriel, S., R. W. Lau, and C. Gabriel, "The dielectric properties of biological tissues: III. Parametric models for the dielectric spectrum of tissues," *Physics and Medicine and Biology*, Vol. 41, 2271–2293, 1996.
20. Veselago, V. G., "The electrodynamics of substances with simultaneously negative values of ε and μ," *Soviet Physics USPEK*, Vol. 10, 509–514, 1968.
21. Pendry, J. B., "Electromagnetic materials enter the negative age," *Physics World*, Vol. 14, 47–51, 2001.
22. Smith, D. R. and N. Kroll, "Negative refractive index in left handed materials," *Physical. Review. Letters*, Vol. 85, 2933–2936,

2000.

23. Smith, D. R., W. J. Padilla, D. C. Vier, S. C. Nermat-Nasser, and S. Schultz, "A composite medium with simultaneously negative permeability and permittivity," *Physical. Review. Letters*, Vol. 84, 4184–4187, 2000.
24. Zainud-Deen, S. H., A. Z. Botros, and M. S. Ibrahim, "Scattering from bodies coated with metamaterial using FDFD method," *Progress In Electromagnetics Research B*, Vol. 2, 279–290, 2008.
25. Valagiannopoulos, C. A., "Electromagnetic scattering from two eccentric metamaterial cylinders with frequency-dependent permittivities differing slightly each other," *Progress In Electromagnetics Research B*, Vol. 3, 23-34, 2008.
26. Ahmed, S. and Q. A. Naqvi, "Electromagnetic scattering of two or more incident plane waves by a perfect electromagnetic conductor cylinder coated with a metamaterial," *Progress In Electromagnetics Research B*, Vol. 10, 75-90, 2008.
27. Yu, G. X. and T. J. Cui, "Imaging and localization properties of LHM superlens excited by 3D horizontal electric dipoles," *J. of Electromagn. Waves and Appl.*, Vol. 21, No. 1, 35–46, 2007.
28. Wang, M. Y., J. Xu, J. Wu, Y. B. Yan, and H. L. Li, "FDTD study on scattering of metallic column covered by double-negative metamaterial," *J. of Electromagn. Waves and Appl.*, Vol. 21, No. 14, 1905–1914, 2007.